Pre-Steady-State Kinetics of Ba-Ca Exchange Reveals a Second Electrogenic Step Involved in Ca^{2+} Translocation by the Na-Ca Exchanger

Andreas Haase and Klaus Hartung*
Max-Planck-Institut für Biophysik, Frankfurt, Germany

ABSTRACT Kinetic properties of the Na-Ca exchanger (guinea pig NCX1) expressed in *Xenopus* oocytes were investigated with excised membrane patches in the inside-out configuration and photolytic Ca^{2+} concentration jumps with either 5 mM extracellular Sr^{2+} or Ba^{2+}. After a Ca^{2+} concentration jump on the cytoplasmic side, the exchanger performed Sr-Ca or Ba-Ca exchange. In the Sr-Ca mode, currents are transient and decay in a monoexponential manner similar to that of currents in the Ca-Ca exchange mode described before. Currents recorded in the Ba-Ca mode are also transient, but the decay is biphasic. In the Sr-Ca mode the amount of charge translocated increases at negative potentials in agreement with experiments performed in the Ca-Ca mode. In the Ba-Ca mode the total amount of charge translocated after a Ca^{2+} concentration jump is ~4 to 5 times that in Ca-Ca or Sr-Ca mode. In the Ba-Ca mode the voltage dependence of charge translocation depends on the Ca^{2+} concentration on the cytosolic side before the Ca^{2+} concentration jump. At low initial Ca^{2+} levels (~0.5 μM), charge translocation is voltage independent. At a higher initial concentration (1 μM Ca^{2+}), the amount of charge translocated increases at positive potentials. Biphasic relaxation of the current was also observed in the Ca-Ca mode if the external Ca^{2+} concentration was reduced to $\leq$0.5 mM. The results reported here and in previous publications can be described by using a 6-state model with two voltage-dependent conformational transitions.

INTRODUCTION

Ca^{2+} concentration and voltage-jump experiments have shown that outward Ca^{2+} translocation by the Na-Ca exchanger NCX1 is coupled to the outward movement of negative charge (1–3). In the Ca-Ca exchange mode, Ca^{2+} concentration jumps performed on the cytoplasmic side of membrane patches (inside-out configuration) excised from guinea pig cardiac myocytes or oocytes containing Na-Ca exchanger NCX1 elicit a transient current (3,4). From the voltage and Ca^{2+} dependence of the relaxation current, it has been concluded that the Ca^{2+} translocating branch of the reaction cycle is described by at least 4 reaction steps or 5 states (see Fig. 8 *A*): electroneutral Ca^{2+} binding reactions on both sides, a fast electrogenic conformational transition, and a slower electroneutral conformational transition after intracellular Ca^{2+} binding (4,5).

To obtain further information on the reaction mechanism of the Na-Ca exchanger, we investigated the kinetics of the exchange of intracellular Ca^{2+} versus those of extracellular Sr^{2+} or Ba^{2+}. It has been shown in previous studies that Sr^{2+} and Ba^{2+} induce Na^+ transport by the exchanger, although at different rates. Sr-Na exchange is as fast as Na-Ca exchange, whereas Ba-Na exchange is much slower (6–9). In the experiments described here, Ba^{2+} or Sr^{2+} were applied on the extracellular side and a Ca^{2+} concentration jump was performed on the cytoplasmic side. Mixed Sr-Ca or Ba-Ca exchange modes were used instead of Ba-Ba or Sr-Sr exchange, because the photolabile chelator DM-nitrophen, which is used to generate concentration jumps, has a relatively low affinity for Ba^{2+} (10). This makes it difficult to perform concentration jumps of sufficient magnitude and to establish a low concentration before the concentration jump (2,11). The affinity of DM-nitrophen for Sr^{2+} is not known, but that of EDTA from which DM-nitrophen is derived is ~2 orders of magnitude lower for Sr^{2+} than that for Ca^{2+} (12).

The amplitude of currents obtained with Ba^{2+} or Sr^{2+} is comparable to that obtained with extracellular Ca^{2+}. In the presence of 5 mM external Ba^{2+}, the decay of the transient current is biphasic, whereas, in the presence of 5 mM external Sr^{2+}, the signal decays in a monoexponential manner (similar to that observed for Ca-Ca exchange with 5 mM extracellular Ca^{2+}). To account for the biphasic decay, the reaction scheme described previously (4) has been expanded to a 6-state scheme with an additional electrogenic transition (see Fig. 8 *B*).

All experiments were performed with deregulated exchangers (13), i.e., regulatory Ca^{2+} binding sites on the cytoplasmic side were removed to investigate transport processes independent of regulatory mechanisms. Current models on the reaction cycle assume that nonoccupied regulatory binding sites shut down transport activity completely rather than slow the reaction cycle (2). In agreement with this idea, we have reported that the time course of current signals induced by Ca^{2+} jumps is not affected by deregulation (3), although the amplitude is increased by deregulation. Thus, it seems that deregulation does not affect the transport cycle.

To trap exchangers in a nontransporting state before the Ca^{2+} concentration jump, it is necessary to keep the Ca^{2+} concentration before the jump as low as possible. If exchangers are not deregulated, part of the exchangers is

Submitted August 28, 2008, and accepted for publication March 17, 2009.

*Correspondence: hartung@mpibp-frankfurt.mpg.de

Editor: Michael Pusch.

0006-3495/09/06/4571/10 $2.00

doi: 10.1016/j.bpj.2009.03.017

inactivated and Ca^{2+} concentration jumps may affect both binding sites. Furthermore, because of the slow reactions at the regulatory binding site, the fraction of inactivated exchangers may be variable before each concentration jump, complicating the analysis, e.g., the concentration dependence of amplitudes.

MATERIAL AND METHODS

Experiments were performed as previously described (3,4). The major difference was that pipette solutions (in mM: 100 LiOH, 15 TEAOH, 5 CsOH, 5 Hepes adjusted with Mes to pH 7.15) contained either 5 mM Ba^{2+} or Sr^{2+} (added as acetate), instead of 5 mM Ca^{2+}. In some experiments, pipette solutions contained 0.1 or 0.5 mM Ca^{2+} and 5 or 10 mM Mg^{2+} (see text for details). mRNA encoding for NCX1 from guinea pig was injected into *Xenopus* oocytes. After 2 days, giant membrane patches (inside out, diameter ~20 μm) were excised from the oocytes (14). Patches were treated for 1 min with a solution containing α-chymotrypsin (1 mg/mL) on the cytosolic side to deregulate the exchanger (13). Ca^{2+} concentration jumps on the cytoplasmic side were performed using the photolabile Ca^{2+} chelator DM-nitrophen (3,15). Ca^{2+} and DM-nitrophen (Calbiochem, Bad Soden, Germany) were added in varying amounts to the bath solution (in mM: 100 LiOH, 15 TEAOH, 5 CsOH, 5 Hepes adjusted to pH 7.15 with Mes) to establish Ca^{2+} concentration jumps of different magnitude. Cl^--free solutions were used throughout to minimize Ca^{2+}-activated Cl^- currents (4). The DM-nitrophen/Ca^{2+} ratio was always close to 1. A XeCl eximer laser (Lextra 50, Lambda Physics, Göttingen, Germany; emission wavelength 308 nm, pulse duration 10 ns) was used to irradiate a quartz cuvette filled with the laser dye BiBuQ (Lambda Physics; emission maximum at 385 nm (4)). The energy of the laser flash was adjusted such that at least 10% of the chelators were photolyzed (>330 mJ/cm^2). Currents were measured with an Axopatch 200A amplifier (Molecular Devices, Sunnyvale, CA) in the capacitive feed-back mode. To eliminate the artifact generated by the discharge of the laser, the reset function of the amplifier (lasting 50 μs), which shortcircuits the input of the amplifier, was activated 22 μs before the laser flash was triggered (3). Integration of current signals was performed by fitting exponential functions with amplitude A_I and time constant τ_i to the current signal. The integral was then calculated using $\Sigma A_i \cdot \tau_i$: one term for the rise of the current and up to two for the decay. Because of the shortcircuiting of the amplifier at the time of the laser flash, some error was introduced into the integration of the current. This error was insignificant at small concentration jumps, i.e., if the rise time of the signal was large, but it increased if the rise time of the current decreased. Assuming that the true rise time is 0, our procedure to fit the rise of the signal with an exponential function underestimated the integral up to 30% at saturating concentration jumps. Because the rise of the current was limited by the photolysis of DM-nitrophen with a time constant ($\tau = 26$ μs (16)) that equaled the initial gap, it was assumed that the integration of the current was not significantly affected by the initial shortcircuiting.

RESULTS

Stationary current

To test the ability of Sr^{2+} and Ba^{2+} to induce stationary Na-Sr or Na-Ba exchange, current pipette solutions with 5 mM Sr^{2+} or Ba^{2+} were used and Na^+ concentration steps were applied on the cytoplasmic side of the membrane. Fig. 1 *A* shows that outward currents generated by the application of 100 mM Na^+ on the cytoplasmic side with Sr^{2+} on the extracellular side are large and comparable to currents obtained with 5 mM extracellular Ca^{2+}(4,14). Only small stationary currents were observed in the presence of extracellular Ba^{2+} (Fig. 1 *B*), in agreement with previous reports (9, but see 8). The transient currents shown in Fig. 1 *B* are solution exchange artifacts.

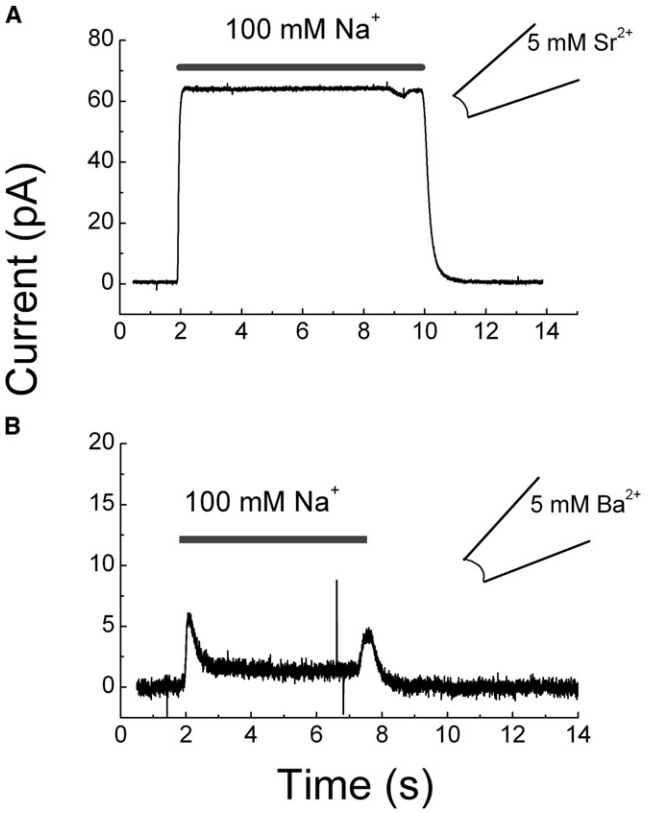

FIGURE 1 Stationary Na-Sr (*A*) and Na-Ba (*B*) exchange current. Inward translocation of Sr^{2+} or Ba^{2+} was activated by applying 100 mM Na^+ on the cytoplasmic side of the membrane patch. The pipette contained either 5 mM Sr^{2+} or Ba^{2+}. Transient currents in *B* are artifacts due to switching of valves.

Pre-steady-state currents

Sr-Ca exchange mode

Fig. 2 *A* shows current records obtained after Ca^{2+} concentration jumps (ΔCa) of different magnitude with 5 mM extracellular Sr^{2+}. As with extracellular Ca^{2+}, the currents were transient, i.e., no stationary current was observed and the decay of the current could be described by a single exponential function (3,4). Fig. 2, *B* and *C* show that the amplitude and the rate constant of decay saturated at large ΔCa. The peak inward current was half-maximal at 97 μM, and the rate constant was half-maximal at 138 μM. The maximal rate constant was ~10,000 s^{-1},which is equivalent to the value in the Ca-Ca mode (4).

Ca^{2+} concentration jumps of different magnitude were also performed at different voltages. Fig. 3, *A* and *B* show current records obtained by Ca^{2+} concentration jumps of 13 μM (*A*) and 545 μM (*B*) at –75, 0, and +75 mV. The amplitude increased at negative potentials at both Ca^{2+} levels, whereas the time course was voltage independent.

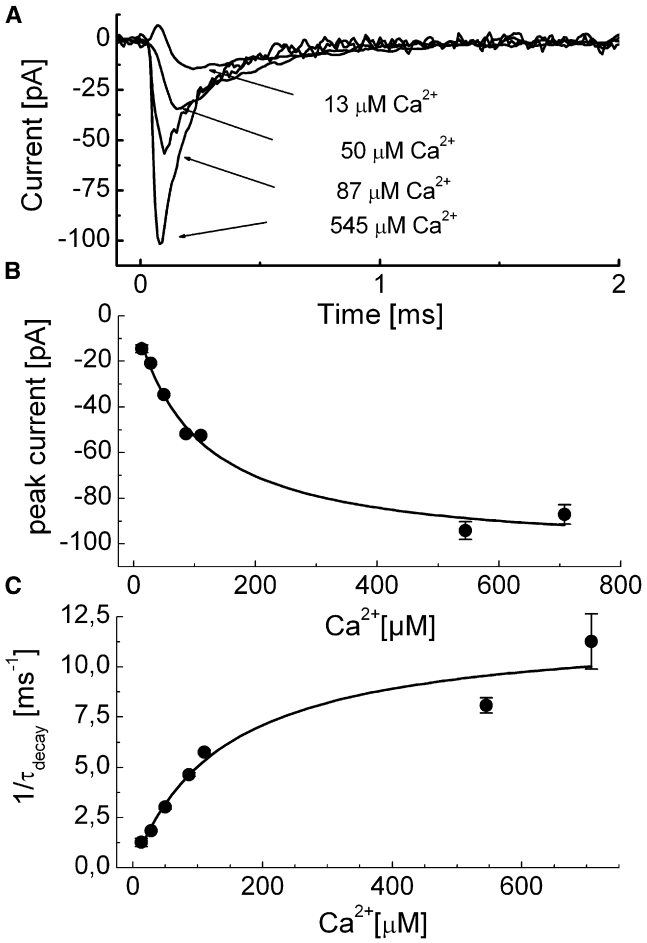

FIGURE 2 Ca^{2+} dependence of prestationary Sr-Ca exchange current. (*A*) Current records obtained after Ca^{2+} concentration jumps of different magnitude. (*B*) Ca^{2+} dependence of the peak current. The continuous line is a Michaelis-Menten fit with $K_m = 97$ μM and $I_{max} = -104$ pA. (*C*) Ca^{2+} dependence of the rate constant of the decay phase of the transient current. A single exponential function was fitted to the decay of the current. The continuous line is a Michaelis-Menten fit, with $K_m = 138$ μM and $1/\tau_{max} = 11990$ s^{-1}.

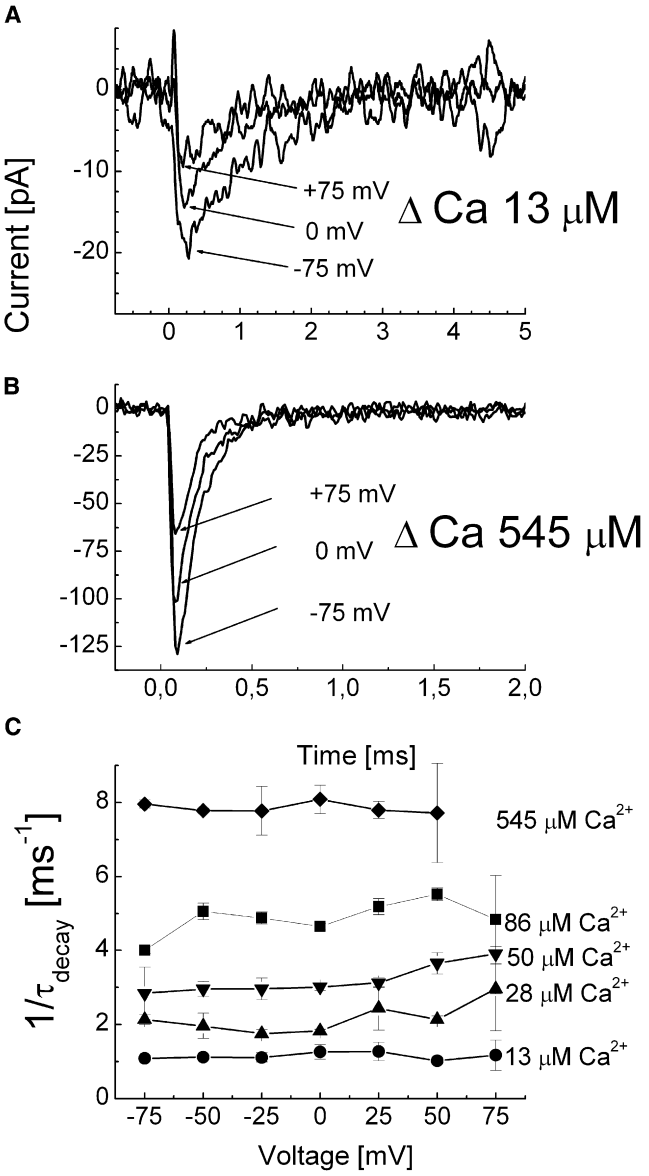

FIGURE 3 Voltage dependence of Sr-Ca exchange currents. Current was elicited by small (13 μM (*A*)) and large Ca^{2+} concentration jumps (545 μM (*B*)) at –75, 0 and +75 mV. (*C*) Voltage dependence of the relaxation rate constant of the decay phase at different Ca^{2+} concentrations.

Fig. 3 *C* demonstrates that the relaxation rate constant of the decay is voltage independent over a large range of Ca^{2+} concentration jumps (10–550 μM). Voltage independence was also observed for the apparent affinities for Ca^{2+} of the relaxation rate constant and of the peak current (Fig. 4, *A* and *B*). Fig. 4, *C* and *D* show the voltage and Ca^{2+} dependence of the charge translocation, i.e., the integrated current signal. In the presence of extracellular Sr^{2+}, the amount of charge translocated increased at negative voltages and was independent of the magnitude of ΔCa at a given voltage between 13 and 545 μM. The slope of the charge-voltage relationship is low: charge changed approximately by a factor of 2 between −75 mV and +75 mV. At 0 mV, the amount of charge translocated is 14.8 ±0.75 fC ($n = 5$). Thus, the charge translocation in the Sr-Ca mode is almost identical to that observed in the Ca-Ca mode (4).

Ba-Ca exchange

External Ba^{2+} catalyzes Ca^{2+} efflux (17) and stationary Ba-Na^+ exchange current (9), but it catalyzes less efficiently than does Ca^{2+} (turnover is 70% lower). If Na^+ or Ca^{2+} binding and translocation are not affected, one has to assume that Ba^{2+} translocation is much slower than Ca^{2+} translocation, limiting the turnover, i.e., the generation of stationary current. Fig. 5 *A* shows a current record obtained after a Ca^{2+} concentration jump (100 μM) on the cytoplasmic side with 5 mM Ba^{2+} in the pipette. Surprisingly, the magnitude of the peak inward current is not much smaller than that under Ca-Ca (4) or Sr-Ca exchange conditions. The decay of the

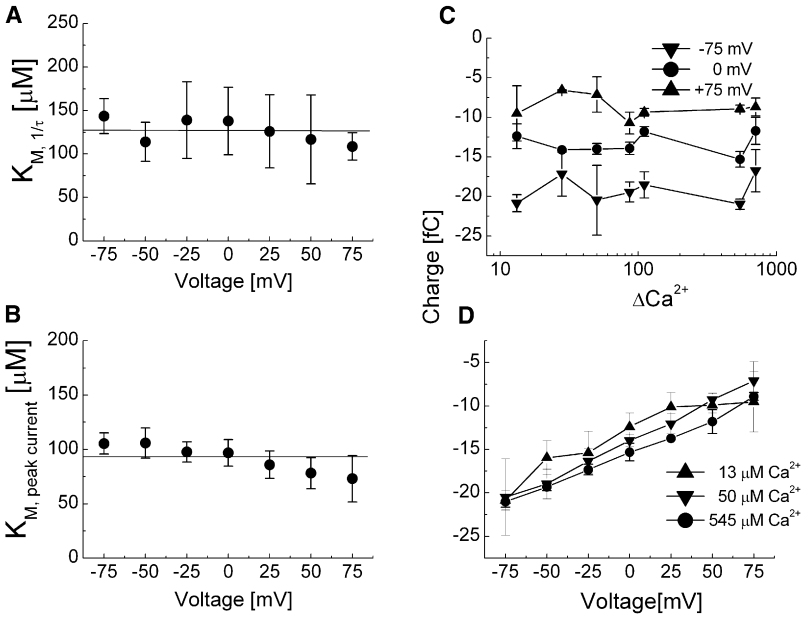

FIGURE 4 Voltage and Ca^{2+} dependence of Sr-Ca exchange current. Voltage dependence of the K_m of the relaxation rate constant (*A*) and of the peak current (*B*). (*C*) Ca^{2+} dependence of charge translocation after Ca^{2+} concentration jumps at different voltages. (*D*) Voltage dependence of charge translocation induced by Ca^{2+} concentration jumps of different magnitude.

current was biphasic, and overall it was much slower than the decay with 5 mM external Ca^{2+} or Sr^{2+} (Fig. 3 *B*) (4). A biexponential fit to the decay yields rate constants of $1/\tau_1 = 4550\ s^{-1}$ and $1/\tau_2 = 450\ s^{-1}$ (Fig. 5 *A*). For comparison, a curve with a monophasic decay is included. In the Ba-Ca exchange mode the voltage dependence of the peak current was variable. Whereas in the Ca-Ca or Sr-Ca exchange mode the peak current increased at negative voltages, the peak current either increased at positive voltages or was almost voltage independent in the Ba-Ca mode. This variability was caused by small variations of the Ca^{2+} concentration before the concentration jump that have no effect in the Ca-Ca or Sr-Ca mode.

This is shown in Fig. 5, *B* and *C*. Currents were obtained from two different membrane patches at negative and positive potentials and two different cytoplasmic Ca^{2+} concentrations before the concentration jump. The magnitude of the concentration jump was 100 μM in both experiments. In Fig. 5 *B* the initial Ca^{2+} concentration was 0.5 μM and the amplitude of the peak current shows no significant voltage dependence, whereas in Fig. 5 *C* the initial Ca^{2+} concentration was 1 μM and the amplitude decreases significantly at negative potentials. Because the time course was almost voltage independent (Fig. 6, *A* and *B*), the same voltage dependence was observed for the integrated current (*charge*). The amount of charge translocated was either voltage independent (Fig. 6 *C*) or increasing at positive potentials (Fig. 6 *D*).

The charge translocated after a Ca^{2+} concentration jump was much larger in the presence of extracellular Ba^{2+} than the charge in the presence of Ca^{2+} or Sr^{2+}: At 0 mV, it was 108 $\pm$ 15 fC ($n = 3$) if the initial Ca^{2+} is $\leq$0.5 μM and 67 $\pm$15 fC ($n = 3$) if the initial Ca^{2+} concentration was 1 μM (cf. Figs. 4, *C* and *D*, and 6, *C* and *D*). About 75% of the charge was related to the slow phase.

Ca-Ca exchange with low extracellular Ca^{2+}

If Ba^{2+} simply acts as a poor substitute for Ca^{2+}, similar results would be expected with small extracellular Ca^{2+} concentrations. Thus, we tried extracellular Ca^{2+} concentrations of 0.1 and 0.5 mM. Unfortunately the success rate was very low under these conditions. In one single experiment a good seal was obtained with 0.1 mM Ca^{2+} and in a few experiments good seals were obtained if 5 or 10 mM Mg^{2+} were added to the pipette solution. However, these seals were not stable enough to apply voltages as in other experiments.

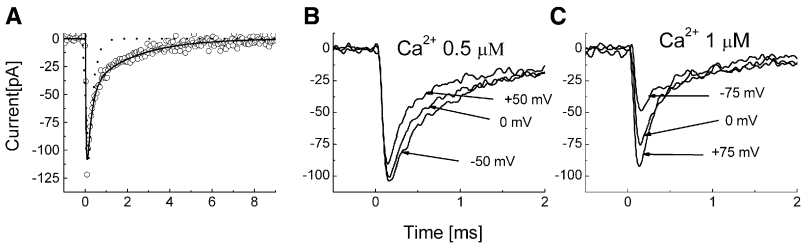

FIGURE 5 (*A*) Current generated by a Ca^{2+} concentration jump (100 μM) with 5 mM Ba^{2+} external (Ba-Ca mode). The data (*o*) were fitted by three exponential functions (—). The decay of the signal is described by two rate constants 4550 s^{-1} and 450 s^{-1}, respectively. For comparison, the dotted line shows a signal with monophasic decay (rate constant 4550 s^{-1}) . (*B* and *C*) Voltage dependence of currents in the Ba-Ca mode. Currents were generated by Ca^{2+}concentration jumps (100 μM) at different holding potentials and initial Ca^{2+} concentrations (0.5 μM and 1 μM).

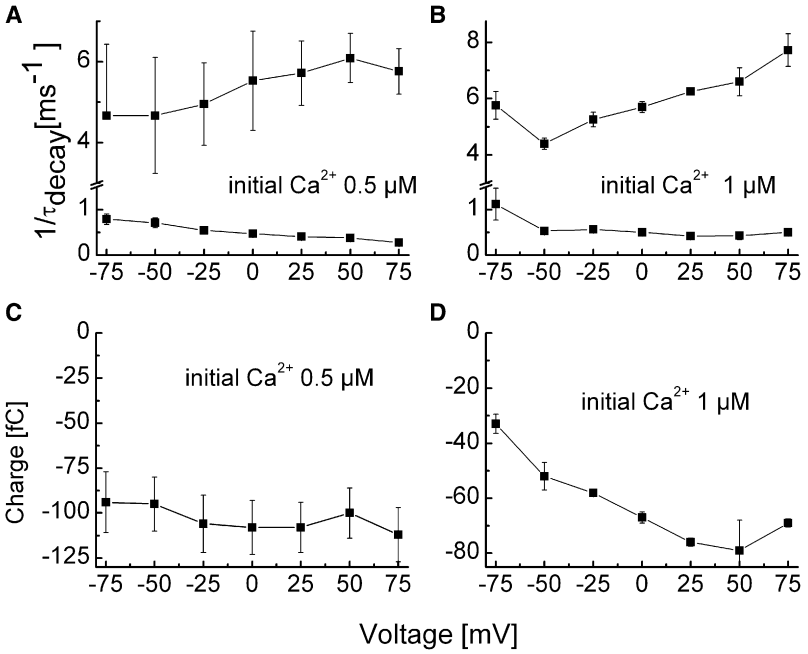

FIGURE 6 Voltage dependence of the relaxation rate constants and of the charge translocation in the Ba-Ca mode as a function of the Ca^{2+} concentration before the concentration jump (0.5 μM in *A* and *C* and 1.0 μM in *B* and *D*). The initial Ca^{2+} level affects mainly the voltage dependence of charge translocation. $\Delta Ca = 100$ μM.

Fig. 7 *A* shows a current record generated by a Ca^{2+} concentration jump (110 μM) with 0.1 mM Ca^{2+} and 10 mM Mg^{2+} in the pipette. A biphasic decay was observed with rate constants ($1/\tau_1 = 8300$ s^{-1} and $1/\tau_2 = 780$ s^{-1}), which are comparable to those obtained in the Ba-Ca mode. Fig. 7 *B* shows an experiment with 0.1 mM external Ca^{2+} without Mg^{2+}. The decay of the signal was also biphasic, but, because the magnitude of ΔCa was not saturating (45 μM), the decay was relatively slow ($1/\tau_1 = 3459$ s^{-1}, $1/\tau_2 = 613$ s^{-1}). Altogether, low external Ca^{2+} induced a biphasic decay of the transient current, and the data support the suggestion that the effects of Ba^{2+} may be mimicked by a low extracellular Ca^{2+} concentration.

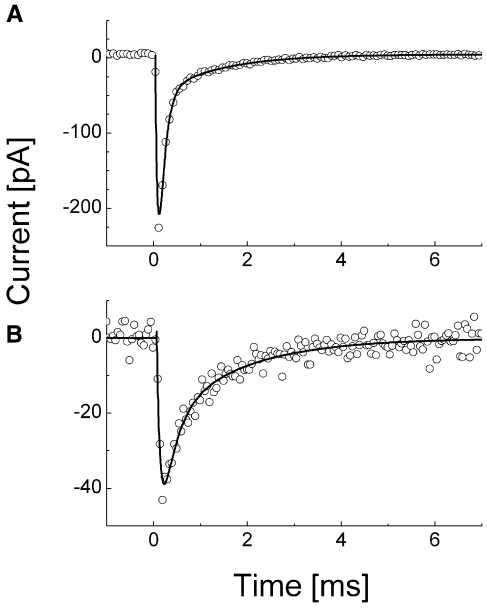

FIGURE 7 Current records obtained in the Ca-Ca mode with low extracellular Ca^{2+} (0.1 mM Ca^{2+}). ΔCa was 110 μM in *A*, and 45 μM in *B*. In *A* the pipette contained 10 mM Mg^{2+} in addition to facilitate seal formation. Open circles: experimental data; continuous line: fit to the data with three exponential functions.

DISCUSSION

Comparison between Ca-Ca and Sr-Ca exchange

Relaxation currents with 5 mM extracellular Sr^{2+} (Sr-Ca exchange) are nearly indistinguishable from currents measured in the presence of 5 mM external Ca^{2+} (Ca-Ca exchange). In both modes a cytoplasmic Ca^{2+} concentration jump elicits a transient inward current that decays monoexponentially (3–5). Also, in both modes the relaxation rate constant is voltage independent but Ca^{2+} dependent, with a maximum of ~10,000 s^{-1} (4). In the Sr-Ca mode the K_m of the rate constant is 138 μM, and that of the peak current is 97 μM compared with 99 and 31 μM under Ca-Ca exchange conditions (4). As in the Ca-Ca mode, the amount of charge translocated is Ca^{2+} independent in the Sr-Ca mode and increases with hyperpolarization (4,5). In both cases the absolute amount of charge translocated is ~15 fC for a patch of ~20 μm diameter at 0 mV. In summary, these measurements confirm previous suggestions derived from Na-Sr exchange that Sr^{2+} is a good substitute for Ca^{2+} (6,8,17,18).

Ba-Ca and Ca-Ca exchange with low external Ca^{2+}

The transient currents induced by Ca^{2+} concentration jumps in the presence of external Ba^{2+} are much larger than expected, considering the low efficiency of Ba^{2+} to induce Ca^{2+} or Na^{+} translocation (9,17). The amplitude of the peak current

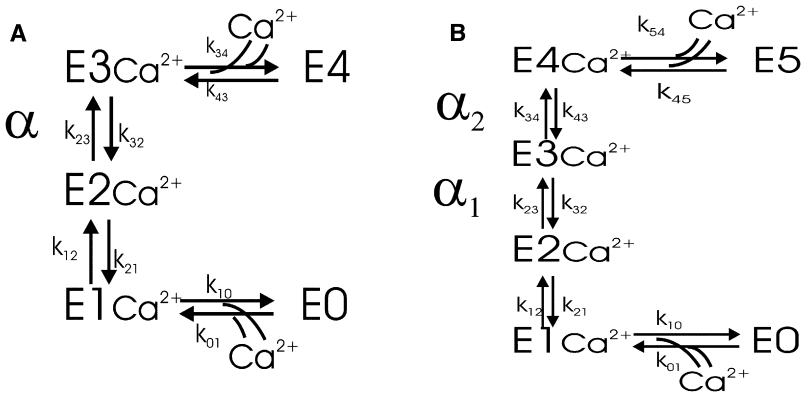

FIGURE 8 Five-state and 6-state reaction models for Ca-Ca exchange (Sr-Ca and Ba-Ca exchange). The 5-state model contains 1 electrogenic transition indicated by the dielectric coefficient α. The 6-state model contains 2 electrogenic transitions indicated by α_1 and α_2. The parameters used to simulate exchanger currents are given in Table 1. E0 designates the empty binding site directed toward the cytoplasma; E4 (*A*) and E5 (*B*) designate the empty binding sites directed to the extracellular space.

is comparable to that measured in the presence of external Ca^{2+} or Sr^{2+}, but the decay phase is biphasic in the Ba-Ca mode. The fast component decays with a rate constant of ~6000 s^{-1} at saturating Ca^{2+} concentrations. This is less than the rate constant observed for Ca-Ca or Sr-Ca exchange but of the same order of magnitude. The second phase, however, decays much slower, with a rate constant of ~300–600 s^{-1}. There may be some voltage dependence of the relaxation rate constants, especially of that of the slow one, but this cannot be said with certainty. Because of the slowly decaying phase, the amount of charge translocated in the Ba-Ca mode is much higher than the amount in the Ca-Ca or Sr-Ca mode. About 75% of the charge translocation is related to the slow phase. The voltage dependence of charge translocation in the Ba-Ca mode is variable and differs from the voltage dependence observed in the Ca-Ca or Sr-Ca mode. In the presence of 5 mM Sr^{2+} or Ca^{2+}, charge translocation increased at negative voltages. In the Ba-Ca mode, voltage independence of charge translocation was observed at low cytoplasmic Ca^{2+} (0.5 μM), whereas an increment at positive voltages occurred if Ca^{2+} was high (1 μM) before the concentration jump.

As shown below, the different forms of voltage dependence can be simulated with the same linear model and parameters by modifying only the cytoplasmic Ca^{2+} concentration before the concentration jump. Furthermore, it is not necessary to introduce additional charges on the transporter to account for the increment of charge translocation observed in the presence of external Ba^{2+}.

Simulations with a 6-state model

Prestationary currents obtained in the Ca-Ca mode could be satisfactorily explained by a 5-state model with one electrogenic transition (E2 ↔ E3, Fig. 8 *A* (cf. ref 4)). To account for the biphasic decay of the transient current, a further electrogenic transition had to be introduced. This transition (E3* ↔ E4*, Fig. 8 *B*) is intercalated between extracellular Ca^{2+} binding and the other electrogenic transition (E2 ↔ E3*). The new transition (E3* ↔ E4*) is marked by asterisks to distinguish it from the E3 ↔ E4 transition in the 5-state model.

In addition to the previous findings (rate constant: Ca^{2+} dependent in a saturating manner and voltage independent; charge translocation: Ca^{2+} independent, voltage dependent (4,5)), the model had to explain two novel observations: 1) the biphasic decay of current observed with extracellular Ba^{2+} or low Ca^{2+}, which was accompanied by charge translocation ~5 times that in the presence of 5 mM Ca^{2+}, and 2) the variability of the voltage dependence of charge translocation in the presence of Ba^{2+} and the discrepancy to the voltage dependence seen in the presence of high Ca^{2+} or Sr^{2+}.

Within the framework of the 5-state model, a dielectric coefficient $\alpha = 0.22$ was assigned to the electrogenic transition (4). For the 6-state model this coefficient was split into $\alpha_1 = 0.16$ and $\alpha_2 = 0.08$. Table 1 shows the rate constants used to simulate the results described above with the 6-state model with external Ca^{2+} and Ba^{2+}. The rate constant of the E4* → E3* transition was high for external Ca^{2+} (10,000 s^{-1}), but low for Ba^{2+} (100 s^{-1}). For the inverse reaction it was identical for both ions (1000 s^{-1}). The other rate constants were identical with those used previously for the 5-state model to simulate Ca-Ca exchange (4).

TABLE 1 Rate constants used to simulate transient currents in the Ca-Ca/Sr-Ca or Ba-Ca exchange mode

		Ca-Ca mode	Ba-Ca mode	Remark
k_{01}	[$M^{-1}s^{-1}$]	1×10^9	1×10^9	According to $K_{D,in} = 0.1$ mM
k_{10}	[s^{-1}]	1×10^5	1×10^5	—
k_{12}	[s^{-1}]	10,000	10,000	—
k_{21}	[s^{-1}]	1000	1000	—
k_{23}	[s^{-1}]	20,000	20,000	$\alpha_1 = 0.16$
k_{32}	[s^{-1}]	25,000	25,000	$\alpha_1 = 0.16$
k_{34}	[s^{-1}]	1000	1000	$\alpha_2 = 0.08$
k_{43}	[s^{-1}]	10,000	100	$\alpha_2 = 0.08$
k_{45}	[s^{-1}]	3×10^6	3×10^6	According to $K_{D,ex} = 3$ mM
k_{54}	[$M^{-1}s^{-1}$]	1×10^9	1×10^9	—

With the exception of k_{34} and k_{43}, the same rate constants were used previously to simulate currents in the Ca-Ca mode with the 5-state model (4). The dielectric coefficient α is a measure for the voltage dependence of rate constant, e.g., $k_{34}(V) = k_{34}(0) * \exp[-\alpha e_0 * V/2kT]$.

Fig. 9 shows simulations of current records obtained with the 6-state model with external Ca^{2+} (5 or 0.1 mM, Fig. 9, *A* and *E*) or 5 mM Ba^{2+} (Fig. 9 *C*) at 0 mV. The simulations yielded transient currents that decayed monoexponentially with 5 mM Ca^{2+} outside but biexponentially with 0.1 mM Ca^{2+} or 5 mM Ba^{2+} outside. Comparison of simulations in Fig. 9 with experimental data in Figs. 3 *B* and 5 shows that the 6-state model reproduces the effect of Ba^{2+} and Ca^{2+} quite well. Simulations with 5 mM external Ca^{2+} are indistinguishable for the 5- or 6-state model. Consideration of the occupation of states before and after ΔCa helps to explain why the relaxation is biphasic with Ba^{2+} or low Ca^{2+} and monophasic with high Ca^{2+}.

Fig. 9, *B*, *D*, and *F* show the calculated distributions of states that underly the simulated currents shown in Fig. 9, *A*, *C*, and *F*. Fig. 9 *B* shows that most exchangers were in state E0, i.e., the empty cytoplasmic binding site, before ΔCa if external Ca^{2+} was 5 mM. After a saturating ΔCa, most molecules were in states E2 and E3*. States E0, E1, E4*, and E5 were almost not populated. Thus, the amount of charge translocated was determined by the E2 ↔ E3* transition, and the other electrogenic transition E3* ↔ E4* did not contribute to the current signal. Because the E2 ↔ E3* transition equilibrated faster (Table 1) than did the E1 ↔ E2 transition, the time course of the decay of the current was mainly determined by the electroneutral E1 ↔ E2 transition if ΔCa was saturating. Below saturation, the time course was determined by electroneutral Ca^{2+} binding. This agrees with the observation of a voltage-independent but Ca^{2+}-dependent relaxation rate constant for the decay of the current (Fig. 3 *C* (4)). In contrast, with Ba^{2+} or low Ca^{2+} on the extracellular side, a large fraction of transporters entered states E*4 and E5 after a saturating ΔCa^{2+}. This is shown in Fig. 9 *D* for a simulated experiment at 0 mV with 5 mM external Ba^{2+} or 0.1 mM Ca^{2+} (Fig. 9 *F*). The initial Ca^{2+} concentration before ΔCa is 0.1 μM and ΔCa was 100 μM. As states E4* and E5 were populated after a saturating ΔCa, both electrogenic transitions contributed now to the current, explaining the increase of charge translocation and the biexponential decay of the current. With respect to Ba^{2+}, this shift of the equilibrium distribution of states was due to the low rate constant for the E4* → E3* transition (Table 1). At low Ca^{2+}, the shift was caused by the reduction of the effective rate of Ca^{2+} binding to the external binding site E5 ($k_{54} \times [Ca^{2+}]_{ex}$). With identical parameters (Table 1), the 6-state model also simulated the different types of voltage dependence of charge translocation observed in the presence of external Sr^{2+}/Ca^{2+} or Ba^{2+}. Most notably, it mimicked the strong effects of small variations of cytoplasmic Ca^{2+} concentrations before ΔCa on the voltage dependence of charge translocation. We discuss first the simulation of the experimental data and then show that the effects can be explained in the framework of the reaction scheme.

Fig. 10 shows the voltage dependence of charge translocation obtained from the simulations with external Ca^{2+} or

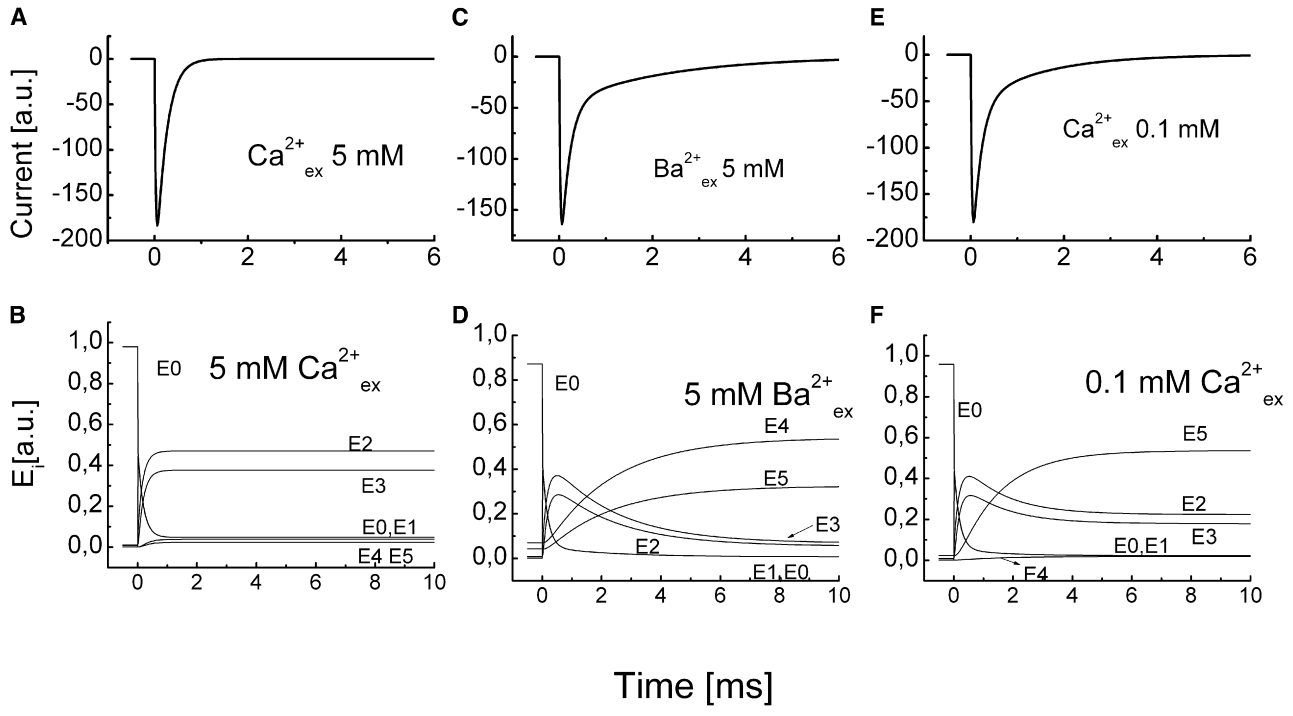

FIGURE 9 Simulation of transient currents and distribution of states with the 6-state model with either 5 mM (*A* and *B*) or 0.1 mM (*E* and *F*) extracellular Ca^{2+} or 5 mM external Ba^{2+} (*C* and *D*). The decay of the current is monoexponential with 5 mM Ca^{2+} and biphasic with 5 mM Ba^{2+} or 0.1 mM Ca^{2+}. The parameters used for the simulation are given in Table 1. Membrane potential was 0 mV. At $t = 0$ the cytoplasmic Ca^{2+} concentration was increased to 0.1 mM.

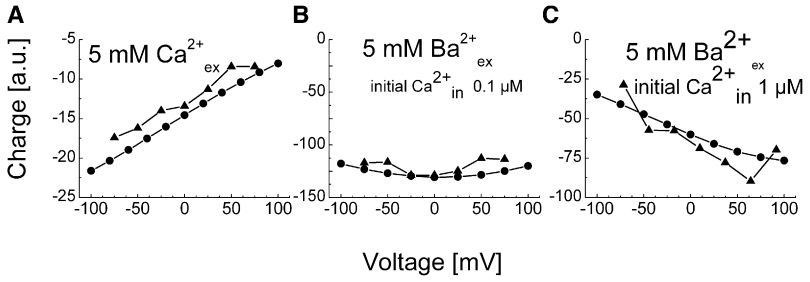

FIGURE 10 Simulation of the voltage dependence of charge translocation with either 5 mM external Ca^{2+} (*A*) or 5 mM Ba^{2+} (*B* and *C*), with initial cytoplasmic Ca^{2+} concentration 0.1 μM (*B*) or 1 μM (*C*). Charge was calculated by integrating simulated current signals. For comparison, experimental data (*triangles*) are included.

Ba^{2+} as discussed above. For comparison, experimental data are included. In the presence of Ba^{2+} two different initial Ca^{2+} concentrations were considered. Currents were calculated with the 6-state model and the parameters given in Table 1. The amount of charge translocated was obtained by integrating simulated current records. Fig. 10 *A* shows that, with 5 mM external Ca^{2+} or Sr^{2+}, the amount of charge translocated increased at negative voltages in agreement with experimental data (4). With 5 mM external Ba^{2+}, charge translocation was either voltage-independent if the initial Ca^{2+} level was low (0.1 μM, Fig. 10 *B*) or it increased at positive voltages (Fig. 10 *C*) if the initial Ca^{2+} level was high (1 μM). This is also in agreement with experimental results. The model also simulated the voltage dependence of the decay time constants of the transient current with external Ba^{2+} and Ca^{2+}/Sr^{2+}. With 5 mM external Ca^{2+}/Sr^{2+}, the decay was monoexponential and the relaxation rate constant showed little voltage dependence (Fig. 11 *A*). At 5 mM external Ba^{2+} or 0.1 mM Ca^{2+}, the decay was biexponential (Fig. 11, *B–D*). The large relaxation rate constant increased slightly at positive voltages, whereas the smaller one decreased as observed experimentally. The relaxation rate constants were independent of the initial Ca^{2+} level.

Initial distribution of states as a determinant of the voltage dependence of charge translocation

After having shown that the 6-state model reproduces the experimental data, it seems appropriate to discuss in more detail how these observations can be explained with one model and by changing only one rate constant. First, the case of 5 mM external Ca^{2+} or Sr^{2+} is considered. Independent of the applied voltage, most exchangers (~90%) were in E0 before ΔCa, i.e., ready to bind Ca^{2+} (Fig. 12, *A* and *B*). The increase of charge translocation at negative voltages observed experimentally was due to the shift of the electrogenic E2 $\leftrightarrow$ E3* transition to E3* at negative voltages. At +100 mV, ~20% of the exchangers were found in E3* after ΔCa (Fig. 12 *A*), compared with ~50% at −100 mV (Fig. 12 *B*). Thus, the fraction of exchangers performing the electrogenic transition E2 $\leftrightarrow$ E3* was larger at −100 mV than at +100 mV, explaining the increase of charge translocation at negative voltages (Fig. 10 *A*). With 5 mM extracellular Ba^{2+} charge, translocation was either voltage independent or increasing at *positive* voltages. It could be shown that the voltage dependence of charge translocation in the presence of external Ba^{2+} is a function of the Ca^{2+} concentration on

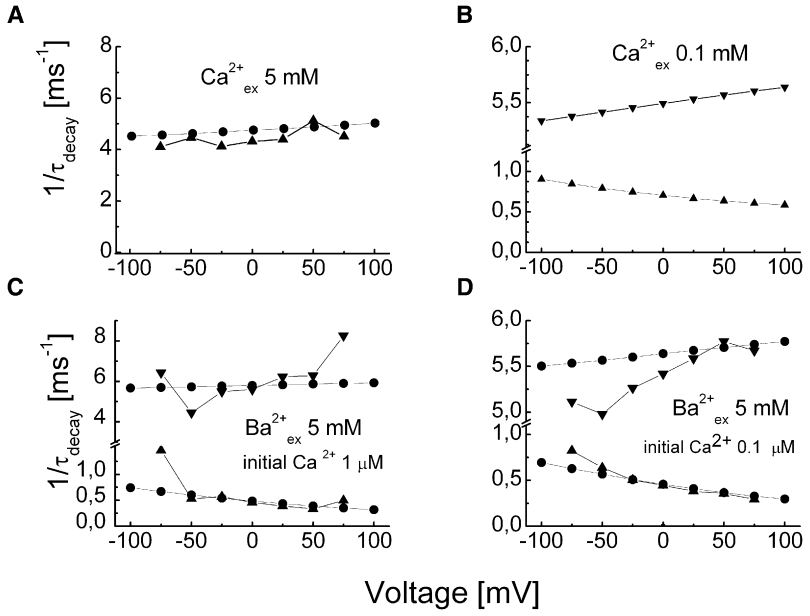

FIGURE 11 Simulation of the voltage dependence of relaxation rate constant (*decay*) for 5 mM external Ca^{2+} (*A*), 0.1 mM external Ca^{2+} (*B*), and 5 mM external Ba^{2+} with either 0.1 μM (*C*) or 1 μM initial Ca^{2+} (*D*). Two or three exponential functions were fitted to currents simulated with the 6-state model. For comparison, experimental data (*triangles*) are included. No experimental voltage dependence is available for *D*.

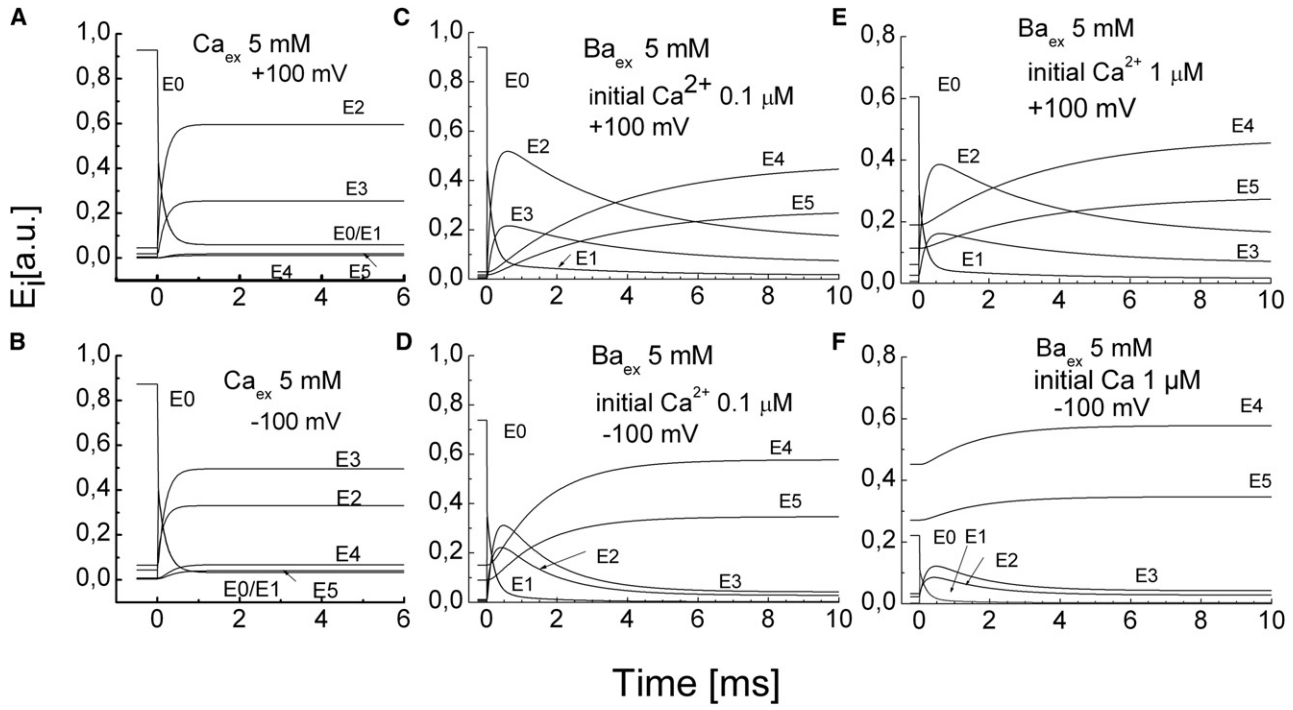

FIGURE 12 Voltage dependence of the distribution of states at +100 and −100 mV before and after ΔCa 100 μM with either 5 mM external Ca^{2+} (*A* and *B*) or Ba^{2+} (*C–F*). (*A*) At −100 mV and 5 mM external Ca^{2+}, more exchangers reach state E3 than at +100 mV, thus increasing the amount of charge translocated at negative voltages. No exchangers enter states E4 and E5. For Ba^{2+} calculations were performed with either 0.1μM (*C* and *D*) or 1 μM cytoplasmic Ca^{2+} (*E* and *F*) before ΔCa. In the presence of Ba^{2+} many exchangers enter states E4 and E5, which explains the increase of charge translocation in the presence of Ba^{2+}. The initial occupation of state E0, E4, and E5 is highly voltage dependent if the initial Ca^{2+} concentration is 1 μM, explaining the voltage dependence of charge translocation.

the cytoplasmic side before ΔCa. This was reproduced by the model without any change of other parameters. The simulations show that, in the presence of external Ba^{2+}, the initial occupation of states E0, E4*, and E5 is rather sensitive to voltage and small changes of Ca^{2+} .

Fig. 12, *C–F* show the occupation of states before and after a concentration jump for two initial cytoplasmic Ca^{2+} concentrations (0.1 and 1 μM) and two different voltages (+100 and −100 mV). In the presence of 1 μM Ca^{2+} and at −100 mV the fraction of exchangers in states E4 and E5 was large already before ΔCa (70%, Fig. 12 *F*). Conversely, only 20% were in E0. Thus, the fraction of exchangers capable to perform the electrogenic transitions was low. Shifting the voltage to +100 mV (Fig. 12 *E*) had dramatic effects on the initial occupation of E0: ~60% were in this state before ΔCa, whereas the fraction in E4* and E5 was reduced to 30%. After ΔCa the fraction of exchangers in E4 and E5 increased only from 73 to 93% at −100 mV, whereas, at +100 mV, the fraction found in E4* and E5 increased from 30 to 70%. Thus, the number of exchangers performing the electrogenic transitions from E0 to E4* was much larger at +100 mV than the number at −100 mV, explaining why charge translocation increases at positive voltages. In contrast, in the presence of a low cytoplasmic Ca^{2+} concentration (0.1 μM), most exchangers were in state E0 between ±100 mV (74–94%) before ΔCa (Fig. 12, *C* and *D*). The fraction reaching states E4* and E5 after ΔCa was more or less voltage independent (~65% at −100 mV and ~61% at +100 mV), i.e., the number of exchangers passing through the electrogenic steps was voltage independent, explaining the voltage independence of charge translocation at a low initial Ca^{2+} concentration.

The model shows that the increase of charge translocation seen in the presence of Ba^{2+} and the variability of the voltage dependence of charge translocation is not caused by a change of the dielectric coefficient, i.e., the number of negative electrical charges translocated in parallel with divalent cations. Rather, all observations can be explained by modifications of the state of the exchanger before the concentration jump and the states reached after the concentration jump. In the presence of high external Ca^{2+}, the initial distribution is not very sensitive to changes of the voltage or small variations of the initial Ca^{2+}concentration on the cytoplasmic side; i.e., most exchangers are in state E0 under all conditions. On the other hand, the high extracellular Ca^{2+} concentration prevents exchangers from reaching states E4* and E5 after ΔCa. Thus, the amount of charge translocated is determined mostly by the voltage dependence of the E2 ↔ E3* transition. In the presence of Ba^{2+} (and low Ca^{2+}), the initial distribution of states is very sensitive to voltage and small variations of internal Ca^{2+}, leading to the variability of the voltage dependence of charge translocation. Furthermore,

states E4* and E5 are populated under these conditions, leading to the biphasic decay of the transient current.

In conclusion, the experiments reported here on the self-exchange of divalent cations show that Sr^{2+} mimics Ca^{2+}. Most interestingly are, however, experiments with external Ba^{2+} that reveal an additional electrogenic transition in the Ca^{2+} translocating branch of the reaction cycle. Similar results were obtained if external Ca^{2+} was reduced far below saturation. All the experimental data, including the variability of the voltage dependence of charge translocation, can be explained by a 6-state model with two electrogenic transitions, assuming that Ba^{2+} affects only one transition.

The authors thank Drs. L. Beaugé (Cordoba, Argentina), C. Bamann, R. Dempski) and J. Rettinger (all Frankfurt, Germany) for critical reading of the manuscript. There are no conflicts of interest.

REFERENCES

1. Niggli, E., and W. J. Lederer. 1991. Molecular operations of the sodium-calcium exchanger revealed by conformation currents. *Nature*. 349:621–624.
2. Hilgemann, D. W. 1996. Unitary cardiac Na^+, Ca^{2+} exchange current magnitudes determined from channel-like noise and charge movements of ion transport. *Biophys. J.* 71:759–768.
3. Kappl, M., and K. Hartung. 1996. Rapid charge translocation by the cardiac Na^+-Ca^{2+} exchanger after a Ca^{2+} concentration jump. *Biophys. J.* 71:2473–2485.
4. Haase, A., P. G. Wood, V. Pintschovius, E. Bamberg, and K. Hartung. 2007. Time resolved kinetics of the guinea pig Na-Ca exchanger (NCX1) expressed in *Xenopus* oocytes: voltage and Ca^{2+} dependence of pre-steady-state current investigated by photolytic Ca^{2+} concentration jumps. *Pflugers Arch.* 454:1031–1042.
5. Kappl, M., G. Nagel, and K. Hartung. 2001. Voltage and Ca^{2+} dependence of pre-steady-state currents of the Na-Ca exchanger generated by Ca^{2+} concentration jumps. *Biophys. J.* 81:2628–2638.
6. Trosper, T. L., and K. D. Philipson. 1983. Effects of divalent and trivalent cations on Na^+-Ca^{2+} exchange in cardiac sarcolemmal vesicles. *Biochim. Biophys. Acta*. 731:63–68.
7. Tibbits, G. F., and K. D. Philipson. 1985. Na^+-dependent alkaline earth metal uptake in cardiac sarcolemmal vesicles. *Biochim. Biophys. Acta*. 817:327–332.
8. Condrescu, M., G. Chernaya, V. Kalaria, and J. P. Reeves. 1997. Barium influx mediated by the cardiac sodium-calcium exchanger in transfected Chinese hamster ovary cells. *J. Gen. Physiol.* 109:41–51.
9. Trac, M., C. Dyck, M. Hnatowich, A. Omelchenko, and L. V. Hryshko. 1997. Transport and regulation of the cardiac Na^+-Ca^{2+} exchanger, NCX1. Comparison between Ca^{2+} and Ba^{2+}. *J. Gen. Physiol.* 109: 361–369.
10. Grell, E., E. Lewitzki, H. Ruf, E. Bamberg, G. C. Ellis-Davies, et al. 1989. Caged-Ca^{2+}: a new agent allowing liberation of free Ca^{2+} in biological systems by photolysis. *Cell. Mol. Biol.* 35:515–522.
11. Zucker, R. S. 1993. The calcium concentration clamp: spikes and reversible pulses using the photolabile chelator DM-nitrophen. *Cell Calcium.* 14:87–100.
12. Anderegg, G. 1977. Critical Survey of Stability Constants of EDTA Complexes. Pergamon Press, New York.
13. Hilgemann, D. W. 1990. Regulation and deregulation of cardiac Na^+-Ca^{2+} exchange in giant excised sarcolemmal membrane patches. *Nature*. 344:242–245.
14. Hilgemann, D. W. 1989. Giant excised cardiac sarcolemmal membrane patches: sodium and sodium-calcium exchange currents. *Pflugers Arch.* 415:247–249.
15. Kaplan, J. H., and G. C. Ellis-Davies. 1988. Photolabile chelators for the rapid photorelease of divalent cations. *Proc. Natl. Acad. Sci. USA*. 85:6571–6575.
16. Ellis-Davies, G. C. R., J. H. Kaplan, and R. J. Barsotti. 1996. Laser photolysis of caged calcium: rates of calcium release by nitrophenyl-EGTA and DM-nitrophen. *Biophys. J.* 70:1006–1016.
17. Blaustein, M. P., and E. M. Santiago. 1977. Effects of internal and external cations and of ATP on sodium-calcium and calcium-calcium exchange in squid axons. *Biophys. J.* 20:79–111.
18. Kimura, J., S. Miyamae, and A. Noma. 1987. Identification of sodium-calcium exchange current in single ventricular cells of guinea-pig. *J. Physiol.* 384:199–222.